J. Fluid Mech. (1971), *vol.* 49, *part* 3, *pp.* 461–479
Printed in Great Britain

An experimental study of peristaltic pumping

By S. L. WEINBERG,† E. C. ECKSTEIN AND A. H. SHAPIRO
Department of Mechanical Engineering, Massachusetts Institute of Technology

(Received 19 January 1971)

An apparatus that approximates a two-dimensional, infinite train of peristaltic waves yields measurements of mean flow, of mean pressure rise, and of pressure-time pulses at fixed locations. In addition, visual observations of 'reflux' and 'trapping', using dyed fluid, are shown. The inertia-free range extends up to a Reynolds number of about 1. In this range, the theory of Shapiro, Jaffrin & Weinberg (1969) is confirmed with respect to mean pressure *vs.* mean flow, pressure *vs.* time, reflux, and trapping. The controversy regarding the criterion of material reflux is settled in favour of the Lagrangian time-mean velocity rather than the Eulerian time-mean velocity. Experiments at higher Reynolds numbers show that the second-order expansion theory of Jaffrin (1971) is valid up to a Reynolds number of about 10.

1. Introduction

The experimental investigations of this paper concern two-dimensional peristaltic pumping with Reynolds numbers ranging from the inertia-free limit to values in which inertial effects are significant.

The governing parameters of the problem

Four dimensionless parameters govern the fluid-mechanical problem of a liquid that is pumped by an infinite train of peristaltic waves of sinusoidal form that progress along the walls of a symmetrical, two-dimensional channel (see figure 1):

(i) The wave-number, $\alpha \equiv a/\lambda$, where a is the mean channel half-width and λ is the wavelength.

(ii) The amplitude ratio, $\phi \equiv b/a$, where b is the wave amplitude. Note that $0 \leqslant \phi \leqslant 1$.

(iii) The Reynolds number, the appropriate form of which for low Reynolds numbers is $R \equiv a^2 c/\lambda\nu$, where c is the wave speed and ν is the kinematic viscosity of an incompressible fluid.

(iv) The flow parameter, $\bar{\mathcal{Q}} \equiv \bar{Q}/ac$, where $\bar{Q}$ is the time-mean volume flow rate between the axis of the channel and one wall, per unit depth normal to the paper.

† Present address: Department of Mechanical and Aerospace Engineering, Washington University, St Louis, Missouri.

Theoretical context of the experiments

Shapiro (1967) solved the case of inertia-free, long-wavelength flow ($R = 0$; $\alpha = 0$) for arbitrary values of ϕ and $\bar{2}$, and gave in explicit algebraic form the linear relationship between mean flow and mean pressure rise.

Burns & Parkes (1967) also assumed inertia-free flow ($R = 0$), but considered finite wavelengths ($\alpha \neq 0$). Their series solution, which gives the mean flow for zero mean pressure rise, is limited to small amplitude ratios ϕ.

Conversely, Hanin (1968) considered long wavelengths ($\alpha = 0$) but admitted arbitrary values of R. His series solution, like that of Burns & Parkes, is for $\phi \ll 1$, and gives the mean flow for zero mean pressure rise.

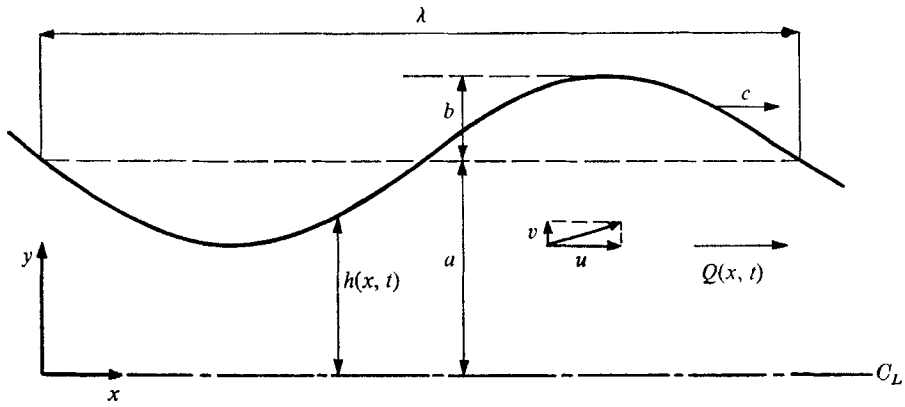

FIGURE 1. Nomenclature for a sinusoidal peristaltic wave.

Fung & Yih (1968) allowed for arbitrary values of R and α, but their solution is limited to small values of ϕ. In one part of the paper, they calculated the Eulerian time-mean velocity at fixed locations and erroneously identified this with the displacement of material fluid. This is a question of potential importance in connexion with so-called 'reflux', i.e. the retrograde passage of bacteria from the bladder to the kidneys, a phenomenon sometimes observed in ureteral function. Fung & Yih concluded that, with a net positive transport of fluid, net negative displacements of fluid, if they occurred at all, would occur at and near the axis of the duct.

In a discussion of Fung & Yih, Jaffrin & Shapiro (1969) argued that, if retrograde motion of fluid is in question, the appropriate quantity to calculate is the Lagrangian displacement of fluid particles, not the Eulerian time-mean velocity. Shapiro *et al.* (1969), in an elaboration and extension of Burnes & Parkes, showed that the Lagrangian mean and the Eulerian mean are often of different sign. Further, they showed that, when reflux does occur, it is near the walls of the tube rather than near the axis. Fung & Yih (1969), in their response to the arguments of Jaffrin & Shapiro, persisted in their position. The mistaken identification of the Eulerian time-mean velocity with the displacement of material particles was again perpetuated by Yin & Fung (1969) and by Zien & Ostrach (1970).

The effects of Reynolds number (inertia) and of wave number (streamline curvature), when these are small but not negligible, were worked out in convenient form by Jaffrin (1971) through expansions in R and α^2, without any limitation on amplitude ratio ϕ.

Latham (1966) presented some experimental results which gave rough confirmation of the inertia-free theory, but his apparatus was not sufficiently precise mechanically to answer many important questions.

Objectives

With reference first to the inertia-free range, $R \ll 1$, there were four objectives: (i) to verify the explicit relationship between time-mean flow and pressure rise per wavelength, given in Shapiro (1967) and Shapiro *et al.* (1969); (ii) to compare experimental curves of pressure *vs.* time at fixed locations with the corresponding theoretical predictions; (iii) to introduce experimental evidence to the theoretical controversy on material reflux, described above; and (iv) to obtain experimental confirmation of the phenomenon of 'trapping' discovered theoretically by Shapiro *et al.* (1969) in which a bolus of fluid in the widest part of the wave is carried along at precisely the wave speed.

In the range where inertia is important, the objectives were (i) to establish up to what value of R the inertia-free theory is valid; (ii) to test Jaffrin's (1971) second-order theory; (iii) to establish up to what value of R the latter is applicable.

2. Experimental apparatus

The flow circuit

The peristaltic pump was located between two open reservoirs, each composed of a lower section (transition chamber) and an open tank of large volume located above it.

The fluid levels within the two reservoirs were controlled by over-flow pipes. Both over-flow pipes were connected to a common sump tank located below the peristaltic pump. A rotary pump supplied liquid from the sump to the upstream reservoir, the level in which was held constant by allowing excess fluid to drain through an over-flow pipe. The level within the downstream reservoir, into which the peristaltic pump discharged, was also controlled by means of an over-flow pipe, in this case an adjustable one. The time-average flow rate was determined by the time required to collect a measured volume of liquid from the downstream overflow pipe. Manometers were used to measure the fluid levels within the reservoirs.

Various mixtures of glycerin and water were used as the working fluid in order to obtain the range of viscosities necessary for wide variations of Reynolds number.

The peristaltic pump

A top view of the peristaltic pump is shown schematically in figure 2. The pumping duct, rectangular in cross-section, was bounded by a rigid semi-circular back wall, a flexible moving wall in which longitudinal waves of transverse displacement were driven by roller cams, and two transparent cover plates.

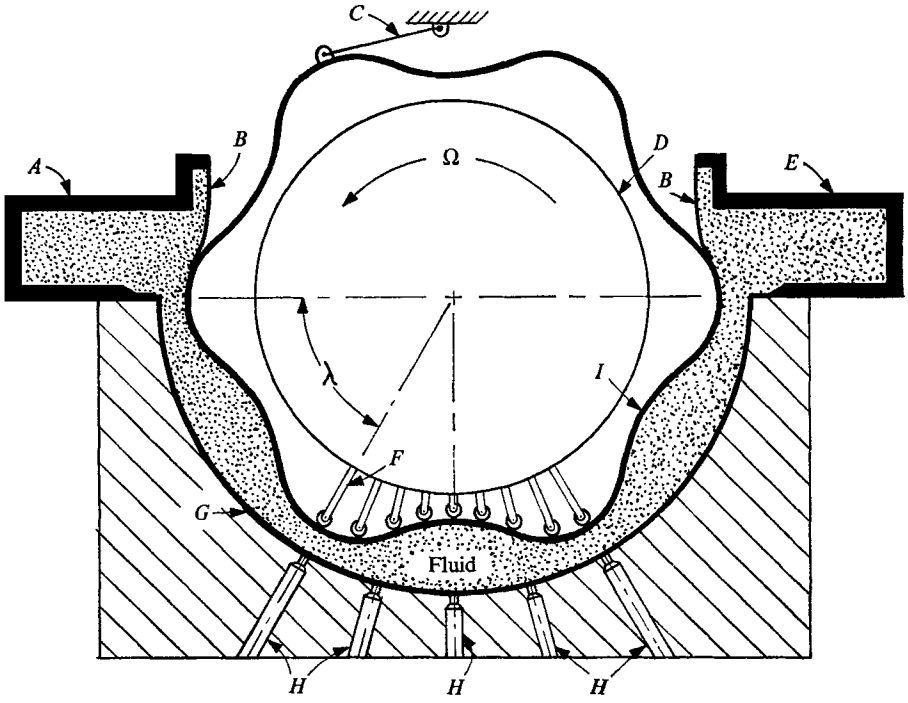

FIGURE 2. Schematic plan view of apparatus. A, upstream transition chamber to reservoir above; E, downstream transition chamber to reservoir above; B, spring steel flaps for sealing; C, cable to restrain rotational motion of moving wall I; D, cam rotor; F, radially-adjustable arms and roller cams; G, semi-circular back wall; H, pressure taps; I, flexible moving wall.

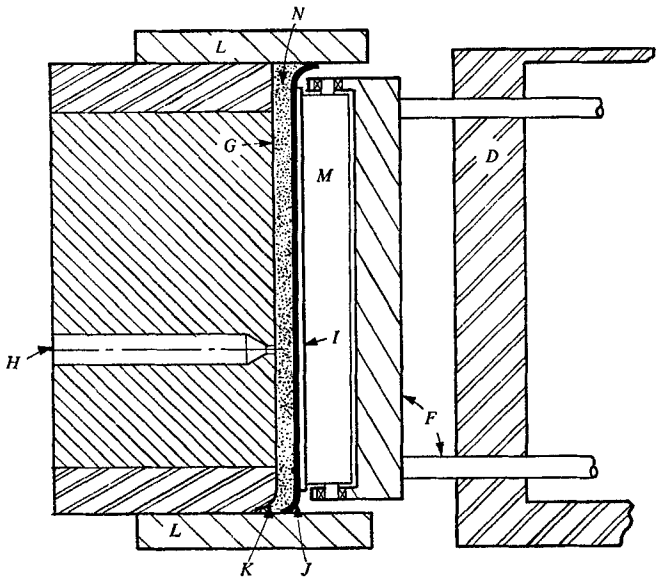

FIGURE 3. Schematic cross-sectional view of apparatus. See also figure 2 for identifying symbols. J, rubber wiper seal; K, seal-recess slot; L, top and bottom cover plates; M, rollers; N, fluid.

Figure 3 shows in cross-section some details of construction. The rectangular duct was 10 in. high, with a mean width ($2a$) of 0·50 in., giving a mean aspect ratio of 20. It was laid out on a semi-circle of radius 17·2 in. Exactly three wavelengths were fitted within the arc length of 54·0 in., so that

$$\lambda = 18{\cdot}0 \text{ in.} \quad \text{and} \quad \alpha = a/\lambda = 0{\cdot}014.$$

The moving wall was composed of a 0·0625 in. thick sheet of 70 durometer rubber attached to a 0·015 in. thick sheet of spring steel. The rubber sheet extended on either side of the steel band, so as to form a wiper seal when installed in the test section. The stationary wall was composed of Plexiglas blocks sandwiched between two aluminium plates. The circular arc was machined into the laminated back wall, then smoothed and polished to be transparent.

Affixed directly to the ends of the backwall were the reservoir transition chambers. The chambers were designed so that a sudden increase in gap width would exist at the termination of the pumping region in order to minimize end effects. These transition chambers also allowed for convenient sealing of the pumping chamber. In the region of the transition chambers spring-steel flaps rested against the moving wall. The rubber sheet referred to above was then attached to these flaps, giving a continuous dynamic seal throughout the pumping chamber. These flaps were clamped to the ends of the transition chambers to form the final seal.

The peristaltic action of the moving wall was produced using a cam assembly to generate a travelling sine wave. The cam assembly was composed of a central rotor, driven by a variable-speed motor, which supported 48 radially adjustable arms on which roller cams were mounted. Thirty of the rollers were aluminium and eighteen were magnetic. The magnetic rollers were used at those wave positions which required a tension force to hold the steel band in position.

Comparison between the experimental design and the two-dimensional theory

In appendix A we show that the infinite periodic wave train of the theoretical literature can be modelled in a finite experiment if certain conditions are met, namely: (i) the peristaltic wave must be progressive and periodic; (ii) there must be an integral number of wavelengths between the reservoirs; (iii) the pressure difference between the reservoirs must be constant.

The apparatus met conditions (i) and (ii) well. However, because of the finite size of the reservoirs and the unsteady character of the flow, the level of each reservoir fluctuated somewhat (a maximum of about 3 mm). In addition, the flaps that were used to seal the transition chambers deformed under static pressure and induced additional pressure fluctuations. These effects were unimportant to the studies at low Reynolds numbers, for which the pressure rise between reservoirs was on the scale of 20 cm. However, the fluctuations in reservoir levels became an appreciable portion of the pressure readings in the experiments at high Reynolds number.

The theories of Shapiro (1967), Burns & Parkes (1967), Hanin (1968), Fung & Yih (1968) and Shapiro *et al.* (1969) refer to a straight pump with two symmetrically moving walls. Mechanically, it is much simpler to construct a duct

laid out on a circular centre-line with one wall stationary. Since the radius of the circle (17·2 in.) in the present experiment was much larger than the mean gap width ($2a = 0{\cdot}5$ in.), the general curvature of the channel was not significant. The very small value of $\alpha = 0{\cdot}014$ signifies that the long-wavelength theory is applicable. Furthermore, when $\alpha \ll 1$, the local pressure gradient is totally determined by the longitudinal variation of total gap width between the two walls; therefore the theory is essentially unchanged by the fact that one wall is rigid and the other moves.

Since the moving wall was indistensible, a small oscillatory longitudinal motion was produced along the wall. Burns & Parkes (1967) have shown that this longitudinal motion has a negligible effect when α is very small, as in the present experiments.

3. Experimental results for inertia-free flow

Mean flow vs. pressure rise

During operation with very small values of R, and with three different amplitude ratios ($\phi = 0{\cdot}4$, 0·7 and 0·9), the dimensionless time-mean flow $\bar{Q}$ was measured as a function of dimensionless pressure rise per wavelength, $a^2\Delta p_\lambda/\mu c\lambda$ (see appendices for nomenclature).

Figure 4 shows typical experimental results for $\phi = 0{\cdot}7$. The experimental results fall on a straight line. Moreover, they show no effects of Reynolds number in the range given, namely, from $R = 0{\cdot}034$ to $R = 0{\cdot}240$. Both these findings confirm that the flow is essentially inertia-free in this range of R, and thus that it corresponds to the limit of zero Reynolds number.

According to the theory of Shapiro *et al.* for $R = 0$, $\alpha = 0$, as summarized in appendix A, the data should follow the solid line of figure 4, representing (A 9). The deviations from the solid line may be accounted for by making two small corrections having to do with departures of the experimental apparatus from the conditions of the simple two-dimensional theory.

One of these departures is that the channel is rectangular in cross-section, rather than two-dimensional. The resulting end-wall effects are rather small, since the depth-width ratio is of the order of 20:1. The method of correcting for the end walls is described in appendix B, and the calculation is made by setting $\mathscr{C} = 0$ in (B 16). This correction alone leads to the dot-dashed line of figure 4. The end walls act to *increase* the zero-flow pressure rise by 1·3 %, and to *decrease* the flow for zero pressure rise by 0·3 %. This may be interpreted by realizing that the purely peristaltic pressure rise associated with zero mean flow is brought about by friction, and that the end walls increase the frictional resistance; but, with a finite mean-flow rate, there is an additional pressure drop associated with and proportional to the frictional resistance of the channel. These two facts together account for the relative positions of the solid line and the dash-dot line of figure 4. Clearly, the end walls have very little effect for the experimental conditions of figure 4 and do not bring theory and experiment together.

It is interesting to note in passing, however, that the average value of $(n+1)/n$ in (B 1) is 1·037, signifying that the end walls would algebraically decrease the

pressure gradient by 3·7 % if the same mean flow were to pass through a uniform duct in which there were no peristaltic waves (the pressure gradient, being negative, would increase in absolute value). This change is quite different from the change shown in figure 4 for either the maximum pressure rise (+1·3 %) or the maximum mean flow (−0·3 %). The explanation, of course, is that $\mathscr{Q}$ in (B 1) has both positive and negative values at different values of $\xi = x/\lambda$; and, moreover, the term H^3 is strongly non-linear. Thus, the substitution in (B 1) of the mean flow and the mean value of H produces a meaningless result.

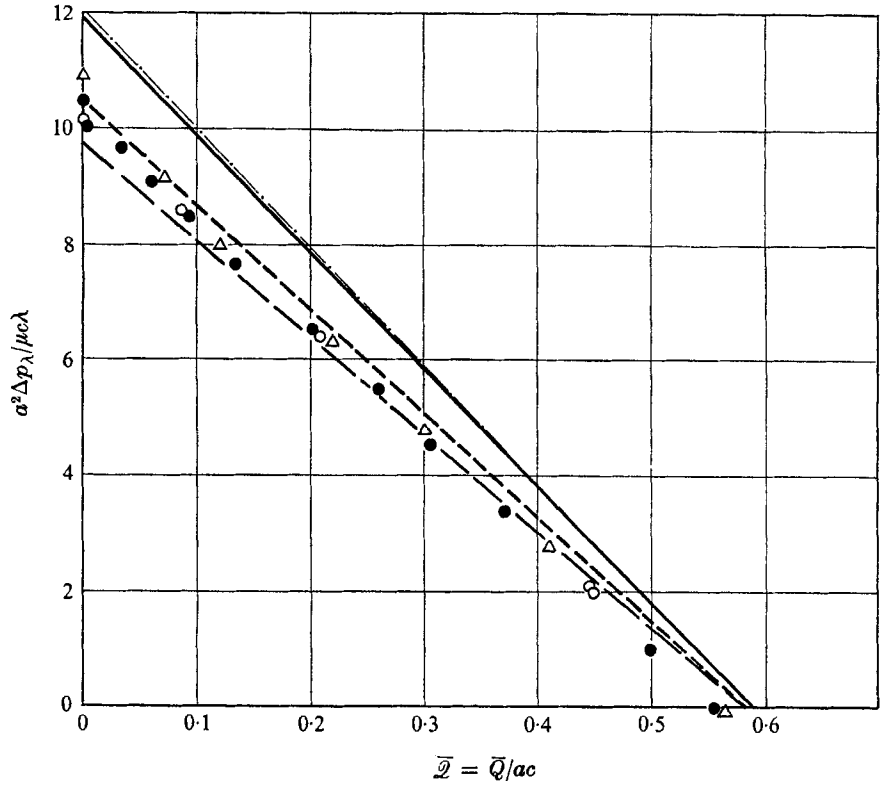

FIGURE 4. Experimental results for $\phi = 0{\cdot}7$, showing dimensionless pressure rise per wavelength *vs.* dimensionless time-mean flow. Note that ordinate is $3\Delta P_\lambda$. ——, two-dimensional theory; —·—·—, two-dimensional theory modified for end walls; – – – –, theory further modified for inactive pumping regions, – – – –, $\mathscr{C} = 0{\cdot}0070$; — — —, $\mathscr{C} = 0{\cdot}0090$ — — —. $R = (ac/\nu).(a/\lambda)$. ○, 0·34; △, 0·070; ●, 0·240.

The second correction to be made is that for back-leakage in so-called 'inactive pumping regions'. These occur in the regions of seal curvature and in the seal-recess slot (see figure 3), where the gap width is much larger than in the channel proper. These regions are relatively ineffective for pumping, since they act somewhat as inactive, or shunt, channels of constant cross-sectional area in parallel with the active peristaltic channel. The method of correcting for the inactive pumping regions is also given in appendix B. It involves a dimensionless conductance parameter $\mathscr{C}$, which depends mainly on the geometry of the inactive channels, and which must be determined empirically.

In figure 4 the two dashed lines were obtained by integration of (B 16) over the interval $\Delta\xi = 1$, using values for the conductance $\mathscr{C}$ of 0·0070 and 0·0090, respectively. The approximate method developed in appendix B for taking account of the inactive leakage area is seen to bring the theory into harmony with the actual circumstances of the experiment. The values of $\mathscr{C}$ mentioned above agree in order of magnitude with the Poiseuille conductance that would be expected of a tube having the dimensions of the inactive leakage area; in this sense, theory and experiment are in good agreement.

For tests with $\phi = 0{\cdot}4$, the value of $\mathscr{C}$ that best fits the data was 0·024. However, because the active channel itself had such a large minimum area in this case the effect of leakage was quite small. As a result, any value of $\mathscr{C}$ between 0·00 and 0·035 produced quite good agreement between theory and experiment. The reason that $\mathscr{C}$ does not remain constant is that it really includes the effects of the resistance to lateral flow in the active channel, and is therefore somewhat dependent upon ϕ.

Pressure–time curves at fixed locations

As shown in appendix A, the pressure should remain constant at integral wavelengths distant from the inlet, and should vary with time between these pressure nodes.

Pressure taps, connected to a differential transducer, were located at distances of 1λ, $5\lambda/4$, $6\lambda/4$, $7\lambda/4$ and 2λ from the beginning of the pumping duct. The pressure differences from the first tap to each of the other taps were traced on a chart recorder.

Figure 5, showing typical results, refers to the case $\phi = 0{\cdot}4$, $\bar{\mathscr{Q}}/\bar{\mathscr{Q}}_0 = 1$, where $\bar{\mathscr{Q}}_0$ is that flow for which there is no mean pressure rise. The four charts refer respectively to the values of $(a^2/\mu c\lambda)\,\Delta p_\lambda$ for distances $\Delta\xi = \frac{1}{4}, \frac{1}{2}, \frac{3}{4}$, and 1. The circles are taken from the experimental traces of pressure *vs.* time, while the curves are calculated theoretically by the methods of appendices A, B, including the corrections for the end walls and for leakage. Since these curves are rather strange in shape, and involve detailed information rather than time or space averages, they provide a very sensitive test both of the validity of the theory and of the experimental procedures. The agreement between theory and experiment is excellent. Pressure pulses measured for $\phi = 0{\cdot}7$ and $\phi = 0{\cdot}9$ also showed good agreement with the theory (Weinberg 1970).

Reflux

Shapiro *et al.* (1969) showed that, when $\bar{\mathscr{Q}}/\bar{\mathscr{Q}}_0 < (2+\phi^2)/3$, the net time-mean flow $\bar{\mathscr{Q}}$ is the algebraic sum of a net forward time-mean flow in the core of the duct and a net retrograde time-mean flow near the walls. Fung & Yih (1968; 1969) Yin & Fung (1969) and Zien & Ostrach (1970), using Eulerian rather than Lagrangian averages, reached an opposite conclusion, namely, that reflux occurs in the core of the duct rather than near the walls.

To observe and document reflux, a neutrally-buoyant dye was injected slowly into the pumping channel midway between the two cover plates that constituted the narrow end walls of the rectangular cross-section. The transverse position of injection within the gap was controlled by a micrometer. A motion-picture

camera mounted directly above the injection port provided visual information as to the displacement history of the dyed fluid.

It was found that, when reflux did occur, it was always near the walls, never near the axis of the channel. This point having been settled, the domain of reflux was most conveniently delineated by depositing the dye very close to one of the walls, since Shapiro *et al.* showed that this is where reflux first appears. Dye near the wall, it was observed, moved alternately forward and backwards. If the dye gradually worked its way upstream, i.e. opposite to the wave direction, it was concluded that reflux occurred, otherwise not.

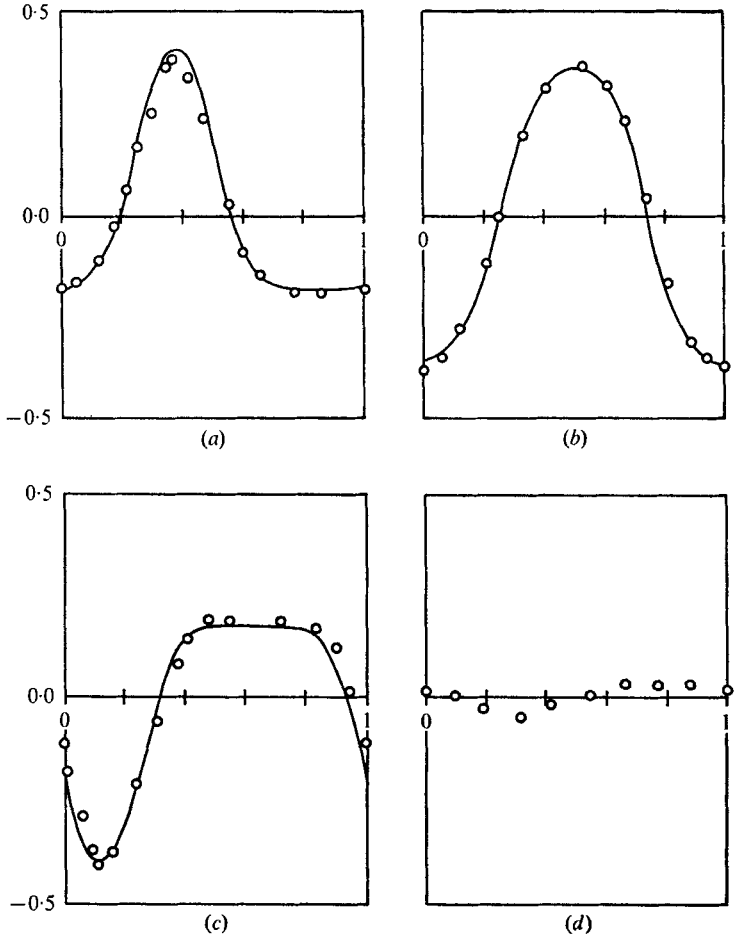

FIGURE 5. Experimental results for $\phi = 0{\cdot}4$, $\overline{\mathscr{Q}}/\overline{\mathscr{Q}}_0 = 1$. Pressure *vs.* time for intervals $\Delta\xi = \frac{1}{4}, \frac{1}{2}, \frac{3}{4}$ and 1 distant from a pressure node. Vertical scale is the dimensionless pressure difference, $3\Delta P = (a^2/\mu c\lambda)\Delta p$. Horizontal scale is the dimensionless time, ct/λ. Curves are from two-dimensional theory modified for end walls and for inactive pumping regions. Δx: (*a*) $\frac{1}{4}\lambda$; (*b*) $\frac{1}{2}\lambda$; (*c*) $\frac{3}{4}\lambda$; (*d*) λ.

Such visual observations were made for values of ϕ of 0·4, 0·7, and 0·9, and over a range of values of $\overline{\mathscr{Q}}/\overline{\mathscr{Q}}_0$. The data are shown in figure 6 together with the theoretical 'limit of reflux' (solid curve), as predicted by Shapiro *et al.*

The conformity of the experimental data to the theoretical curve, coupled with the observation that reflux first occurs near both walls, is decisive proof that the condition of reflux is determined by the sign of the Lagrangian time-mean velocity rather than of the Eulerian time-mean velocity.

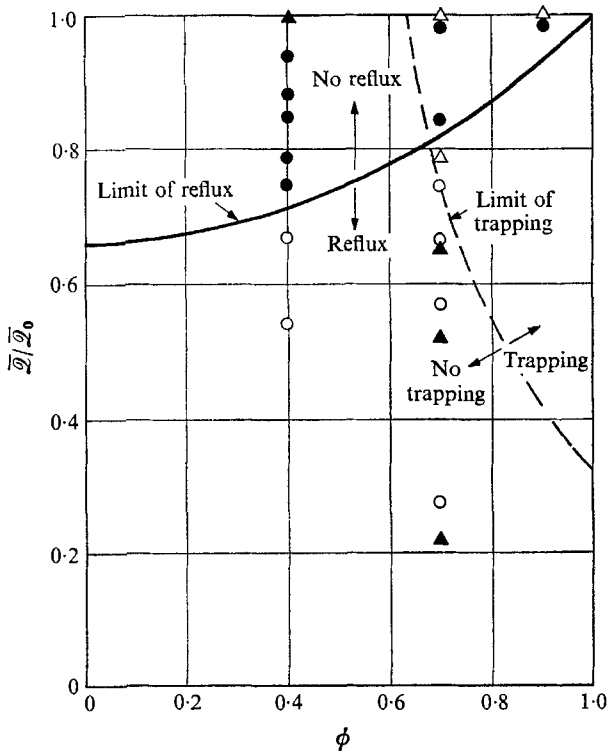

FIGURE 6. Map of $\bar{\mathscr{Q}}/\bar{\mathscr{Q}}_0$ *vs.* ϕ, showing regions of reflux and of trapping. Data points are based on visual observations of whether or not reflux or trapping occurs (see Weinberg). ●, no reflux; ○, reflux; ▲, no trapping; △, trapping.

Trapping

In a frame of reference moving with the wave, the flow is steady. Accordingly, as viewed in the wave frame, the path lines, the streamlines and the streak lines are all coincident. Usually these streamlines are similar to the wall shape, but with decreasing amplitude as the axis is approached. For a certain domain of ϕ and $\bar{\mathscr{Q}}/\bar{\mathscr{Q}}_0$, however, Shapiro *et al.* have shown that the central streamline splits at a stagnation point and encloses a region of recirculating closed streamlines. This region contains, as it were, a bolus of fluid, within which there are internal circulations, but which as a whole remains 'trapped' within the widest part of the channel. In the laboratory frame of reference the bolus moves exactly with the wave speed.

Trapping can be conveniently recognized only when the flow is observed in the wave reference frame. To this end, a movie camera was mounted to rotate with the central shaft of the apparatus, and with the lens directly above a

position of maximum channel width. In the successive frames of film, the channel shape appears stationary and the fluid streams through the channel.

Two procedures for determining the existence of trapping were used (see figure 7). In one, a blob of dye is injected into the channel at a position of minimum gap width. With no trapped bolus, the dye streams through the channel and ultimately disappears from view. With a trapped bolus present, the line of dyed fluid cannot penetrate into the region of closed streamlines. One particle of the dyed fluid approaches asymptotically the stagnation point, where the central streamline splits, while the remainder of the dyed fluid line deforms in such a way as to approach asymptotically the split streamline, and thereby render the latter visible. Figure 8 (plate 1), consisting of a series of movie frames, illustrates such observations for the case $\phi = 0{\cdot}7$, $\bar{Q}/\bar{Q}_0 = 1$.

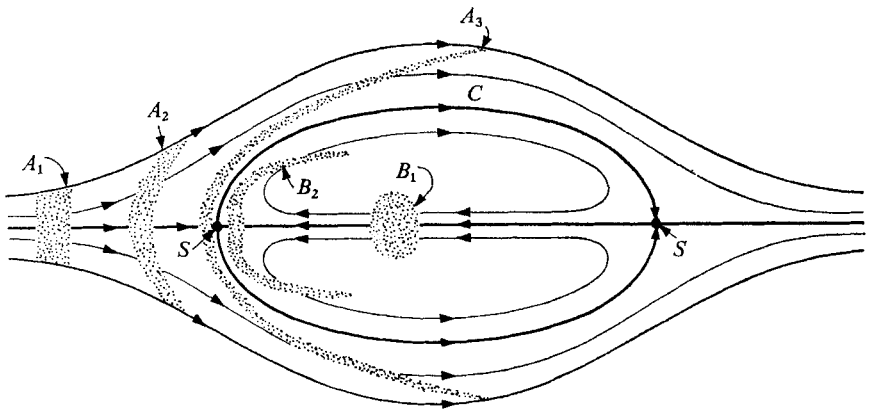

FIGURE 7. Schematic of wave-frame streamlines when trapping occurs. A_1, A_2, A_3 show successive positions of dyed fluid that is injected *outside* the trapped bolus. B_1, B_2 show successive positions of dyed fluid that is injected *inside* the trapped bolus. S represents stagnation points. C represents split streamline that encloses trapped bolus.

In the second method of observation (see figure 7), a blob of dye is injected into the channel near the axis at a position of maximum gap width. Without trapping, the dye is swept out of the field of view. With trapping, the dye moves on the internal closed streamlines within the bolus; that part of the dye close to the axis tends to approach and render visible the split stagnation streamline. The results of such observations are shown in the still views of figures 9(*a*)–(*c*) (plate 2).

Using the foregoing procedures, the presence or absence of trapping was observed for $\phi = 0{\cdot}4$, $0{\cdot}7$ and $0{\cdot}9$, and over a range of values of $\bar{Q}/\bar{Q}_0$. The data are shown in figure 6, where it is seen that they confirm the theoretical predictions of Shapiro *et al.* (1969) for the domain in which trapping occurs.

In photographs of the type of figure 8, the dyed fluid particle on the central axis of the duct could be readily identified because its velocity approached zero as it neared the stagnation point. By measuring the displacement of this stagnation particle as a function of time, the normalized wave-frame velocity $\hat{u}/c$ on the axis could be determined quantitatively as a function of position x/λ. The

experimental results, shown in figure 10, are in good agreement with the theory of Shapiro *et al.*

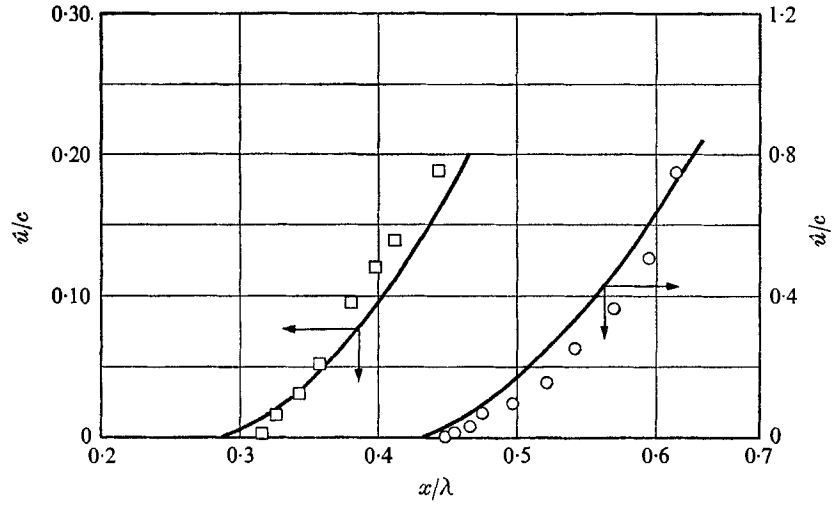

FIGURE 10. Velocity (as seen in wave frame) on stagnation streamline, *vs.* wave-frame position. Data points are from displacement measurements made on photographs like figure 8. Curves are from two-dimensional theory of Shapiro *et al.* (See Weinberg 1970.) □, $\phi = 0{\cdot}7$, $\bar{2}/\bar{2}_0 = 0{\cdot}7$; ○, 0·7, 1.

4. Experimental results: effects of Reynolds number

The Reynolds number was varied by using fluids of different viscosity, and by changes of wave speed. A range of R between 0·008 and 31 was attained, spanning more than 3 decades. For practical reasons, tests at the higher Reynolds number could be made only with $\phi = 0{\cdot}7$.

For any particular Reynolds number beyond the inertia-free range, only a small departure from linearity appeared in the curves of ΔP_λ *vs.* $\bar{2}$. Accordingly, the results are conveniently represented in terms of $\Delta p_{\lambda,\max}$ (for $\bar{2} = 0$), and $\bar{2}_0$ (for $\Delta p_\lambda = 0$).

These are plotted *vs.* R in figures 11, 12. The solid curve in each graph is the expansion solution of Jaffrin (1971) up to terms of order R^2. The dashed line in each graph shows the zero-Reynolds limit after modification for the effects of the end walls and the inactive pumping regions.

Figure 11, showing $\Delta p_{\lambda,\max}$, indicates that the inertia-free theory remains valid up to $R \cong 1$, and that Jaffrin's second-order expansion is valid up to $R \cong 10$.

Figure 12 shows $\bar{2}_0$ *vs.* R, but there is more uncertainty in these results. Since the pressure rise within the apparatus was relatively small at high R (because of the low viscosity), the fluctuations in reservoir level introduced relatively large errors when operating with nominally equal reservoir levels ($\Delta p_\lambda = 0$). Thus, while the experimental observation of $\Delta p_{\lambda,\max}$ was in general very accurate, owing to the ease of establishing the no-flow condition, the experimental observation of $\bar{2}_0$ at high R involved errors which are estimated as being at most ± 5 % for the

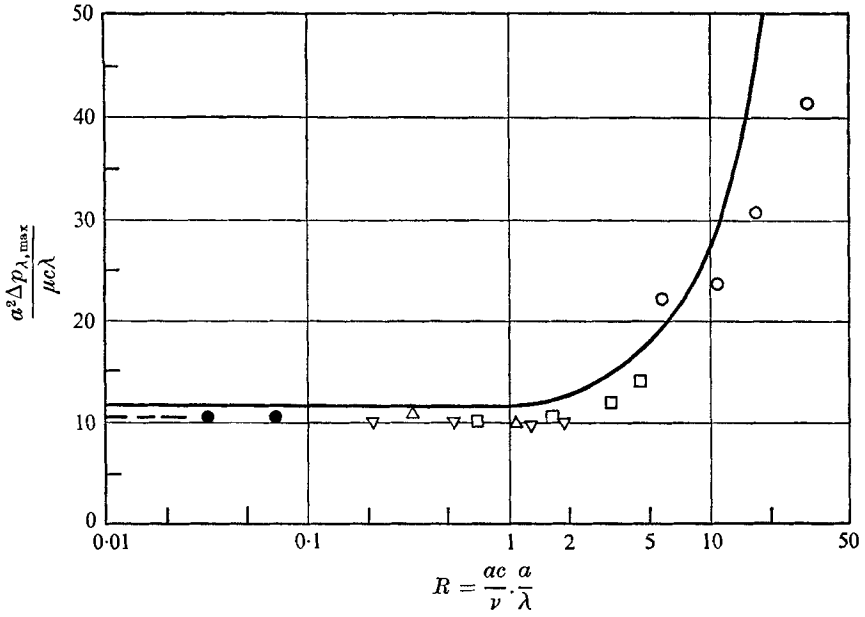

FIGURE 11. Effect of Reynolds number on maximum pressure rise. Ordinate shows dimensionless pressure rise, $3\Delta P_{\lambda,\max}$, for $\bar{Q} = 0$. Data points are from experiments with $\phi = 0{\cdot}7$. Solid curve is theory based on second-order expansion in R. Dashed line is inertia-free theory corrected for end walls and inactive pumping regions. (See Eckstein 1970.) Viscosity: ○, 1 cp; □, 6; ▽, 12; △, 14; ●, 150.

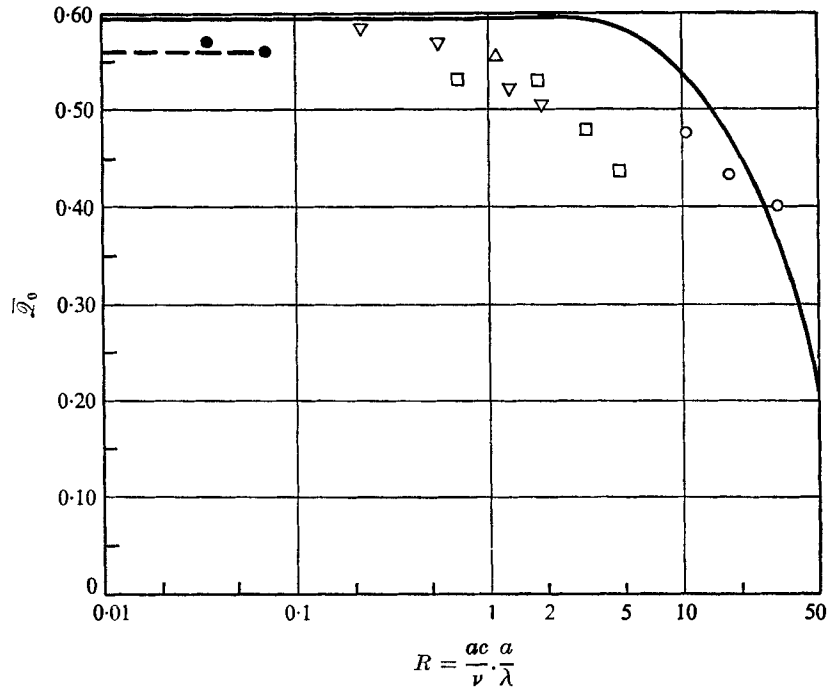

FIGURE 12. Similar to figure 11, but showing $\bar{Q}_0$ *vs.* R, with $\phi = 0{\cdot}7$. (See Eckstein 1970.)

data points of figure 12. Upon making allowance for the added experimental errors, however, we see that figure 12 confirms the conclusions reached on the basis of figure 11.

5. Conclusions

(i) The inertia-free theory is valid up to $R \cong 1$.

(ii) The theoretical predictions of Shapiro *et al.*, concerning reflux and trapping in the inertia-free range, are confirmed by the experiments. The phenomenon of reflux is determined by the sign of the Lagrangian time-mean velocity rather than of the Eulerian time-mean velocity.

(iii) The second-order expansion in R is valid up to $R \cong 10$.

This paper is based on the Doctoral thesis of S. L. Weinberg and on the Master's thesis of E. C. Eckstein. The work on which the paper is based was supported in part by Fluid Dynamics Branch, Office of Naval Research, under contract N00014-67-A-0204-0008, NR 062-400/1-11-67.

Appendix A. Modelling of an infinite two-dimensional wave train

An infinite wave train is clearly not practical for experimentation, except for the special case where it is closed upon itself, and thus transports fluid without net pressure rise. We accordingly seek the circumstances under which an experiment with a finite number of waves does indeed represent the infinite wave train which is the subject of almost all the theoretical literature.

Continuity

We consider the flow as seen in the laboratory reference frame (see figure 1). Let $u(x, y, t)$ be the longitudinal velocity, $p(x, t)$ the pressure over each section, $h(x, t)$ the lateral distance from the axis to the wall, t the time, and $Q(x, t)$ the instantaneous volume flow (per unit width normal to the paper) between the axis and the wall. Then, in terms of the normalized variables,

$$\xi \equiv x/\lambda, \quad \tau \equiv ct/\lambda, \quad \mathscr{Q}(\xi, \tau) \equiv Q/ac \quad \text{and} \quad H(\xi, \tau) \equiv h/a,$$

the equation of continuity of an incompressible fluid is written as

$$\partial \mathscr{Q}/\partial \xi + \partial H/\partial \tau = 0. \tag{A 1}$$

We suppose that the peristaltic wave in the wall is progressive, i.e.

$$H(\xi, \tau) = H(\xi - \tau).$$

Accordingly, $\partial H/\partial \tau = -H' = -\partial H/\partial \xi$ where H' signifies the derivative of the function with respect to the argument $(\xi - \tau)$. Then (A 1) becomes

$$\partial \mathscr{Q}/\partial \xi = \partial H/\partial \xi. \tag{A 2}$$

Upon integration with respect to ξ at constant τ, we get

$$\mathscr{Q}(\xi, \tau) = H(\xi - \tau) + f(\tau), \tag{A 3a}$$

where $f(\tau)$ is a constant of integration that depends upon time. The physical meaning of $f(\tau)$ becomes apparent when we consider that the instantaneous flow in the laboratory frame is

$$Q = \int_0^h u\,dy,$$

while the instantaneous flow in a frame of reference that moves with the wave (the wave-frame) is

$$\hat{Q} = \int_0^h (u-c)\,dy.$$

This shows that $\hat{Q} = Q - ch$, or, in dimensionless terms, $\hat{\mathscr{Q}} = \mathscr{Q} - H$; (A 3$a$) then reveals that $f(\tau)$ is identical with the dimensionless volume flow rate $\hat{\mathscr{Q}}(\tau)$ as seen in the wave frame.

The time-mean flow $\bar{\mathscr{Q}}$ during one period, at a fixed location, may now be expressed with the help of (A 3a) as

$$\bar{\mathscr{Q}} \equiv \int_0^1 \mathscr{Q}(\xi,\tau)\,d\tau = \bar{H} + \int_0^1 \hat{\mathscr{Q}}(\tau)\,d\tau, \tag{A 3b}$$

where $\bar{H}$ is the time-mean value of H.

Navier–Stokes equation

For long wavelengths, $\lambda \gg a$, the pressure is instantaneously uniform over each cross-section; that is, $p(x,y,t) = p(x,t)$. For very low Reynolds number, such that the flow is inertia-free, the longitudinal pressure gradient $\partial p/\partial x$ is balanced by the net viscous force per unit volume. For long wavelengths, the latter is $\mu\,\partial^2 u/\partial y^2$. Thus, a balance of forces yields $\partial p(x,t)/\partial x = \mu\,\partial^2 u/\partial y^2$. Integrating this twice with respect to y at constant x and t, and using the boundary conditions that (i) $\partial u/\partial y = 0$ at $y = 0$, and (ii) $u = 0$ at $y = h$, one gets for $u(x,y,t)$ a local Poiseuille parabolic velocity distribution in terms of the instantaneous local pressure gradient. Then, integrating

$$\int_0^h u\,dy$$

over the cross-section for the flow Q, one gets Poiseuille's law locally in the form,

$$\partial P/\partial \xi = -\mathscr{Q}(\xi,\tau)/H^3, \tag{A 4}$$

where $P \equiv a^2 p/3\mu c\lambda$ is the dimensionless pressure.

Substitution for $\mathscr{Q}$ from (A 3a) then leads to

$$\frac{\partial P}{\partial \xi} = -\frac{1}{H^2} - \frac{\hat{\mathscr{Q}}(\tau)}{H^3}. \tag{A 5}$$

Now consider a machine of dimensionless length $\mathscr{L}$, in which fluid is pumped by means of a peristaltic wave from a reservoir at the pressure $P_1(\tau)$ to a reservoir at the pressure $P_2(\tau)$. Let the pressure difference $P_2 - P_1$ be denoted by $\Delta P_{\mathscr{L}}(\tau)$. Integration of (A 5) with respect to ξ, with τ held constant, yields

$$\Delta P_{\mathscr{L}}(\tau) = -\int_0^{\mathscr{L}} \frac{d(\xi-\tau)}{H^2} - \hat{\mathscr{Q}}(\tau)\int_0^{\mathscr{L}} \frac{d(\xi-\tau)}{H^3}, \tag{A 6}$$

where we have replaced $d\xi$ by $d(\xi-\tau)$, since τ is constant during the integration.

Simulation of an infinite wave train

We have already postulated a periodic travelling wave of the general form $H(\xi-\tau)$. Therefore, if $\mathscr{L}$ is an integral number of wavelengths, each of the integrals in (A 6) is independent of time. If, further, the pressure rise $\Delta P_{\mathscr{L}}$ between the reservoirs is maintained constant, (A 6) shows that $\hat{\mathscr{Q}}(\tau)$ reduces to a constant, independent of time. This means that the flow, in all its details, is steady in the wave frame of reference. Furthermore, examination of (A 3a) shows that $\mathscr{Q}(\xi,\tau) = \mathscr{Q}(\xi-\tau)$, i.e. the flow as seen in the laboratory frame exhibits travelling-wave behaviour; and, concomitantly, from (A 4) or (A 5), the pressure gradient $\partial P/\partial\xi$ is also a function only of $(\xi-\tau)$.

Now all the properties listed above are precisely those which the various theoretical investigations ascribe to an 'infinite wave train'. Indeed, we have here described with precision what this phrase means. To realize such a situation experimentally requires (i) a periodic travelling wave in H, (ii) an integral number of wavelengths between reservoirs, and (iii) a pressure difference between the reservoirs that does not change with time.

Theoretical relation between pressure rise and mean flow

Suppose that we have indeed fulfilled the foregoing conditions to simulate an infinite wave train, such that $\hat{\mathscr{Q}}$ is constant. Then, from (A 3b) and (A 4),

$$\hat{\mathscr{Q}} = \mathscr{Q}(\xi-\tau) - H(\xi-\tau) = \bar{\mathscr{Q}} - \bar{H}, \tag{A 7}$$

where $\bar{\mathscr{Q}}$ is now the same for all periods. Using (A 7), (A 5) may now be expressed as

$$\frac{\partial P}{\partial \xi} = \frac{\bar{H}-\bar{\mathscr{Q}}}{H^3} - \frac{1}{H^2}. \tag{A 8}$$

Since the number of waves is integral and the flow and pressure gradient are periodic, it is convenient to integrate (A 8) over one wavelength, i.e. from $\xi = 0$ to $\xi = 1$. Upon assumption of a sinusoidal wave form, $H = 1+\phi\sin 2\pi(\xi-\tau)$, and noting that $\bar{H} = 1$, integration of (A 8) yields

$$\Delta P_\lambda = \frac{1}{2}\frac{\phi^2}{(1-\phi^2)^{\frac{5}{2}}}\left[3 - \frac{2+\phi^2}{\phi^2}\bar{\mathscr{Q}}\right] \tag{A 9}$$

for the dimensionless pressure rise per wavelength.

Pressure vs. time at fixed locations

We now consider the pressure–time relationship, $P(\tau)$, at a fixed location ξ, since this is one of the measurements easily made as a check on the theory.

We return to (A 8) and integrate it from the inlet reservoir at $\xi = 0$, where P_1 is constant, to any location ξ, where P has the value $P_\xi(\tau)$,

$$P_\xi(\tau) - P_1 = (\bar{H}-\bar{\mathscr{Q}})\int_{-\tau}^{\xi-\tau}\frac{d(\xi-\tau)}{H^3} - \int_{-\tau}^{\xi-\tau}\frac{d(\xi-\tau)}{H^2}. \tag{A 10}$$

First we note that, if ξ is an integer, each of the integrals is a constant, independent of time. Thus, the value of P_ξ at any integral wavelength from the inlet $\xi = 1, 2, \ldots,$

is a constant, independent of time. The integral wavelength positions are therefore nodal points for the pressure.

If ξ is non-integral, the shape of the fractional wavelength momentarily occupying the length ξ will change with time. Mathematically, each integral of (A 10) will depend upon τ, and thus P_ξ will be a function of time. Therefore, if P_1 is interpreted as representing the constant pressure at one of the nodal points, (A 10) yields $P_\xi(\tau)$ at any position between that nodal position and the next one.

Appendix B. Corrections for end walls and for inactive leakage area

The theory of appendix A neglects two effects present in the experiments. Approximate corrections may be developed for these, as shown below.

First, appendix A deals with a purely two-dimensional flow having an infinite aspect ratio $w/2h$, where w is the depth of the channel normal to the paper and $2h$ is the local total width of channel. The aspect ratio of the experiments is variable, but is of the order of 20:1; this turns out to be large enough for the flow to be affected only slightly by the end walls. Purday (1949) provides a good approximation to the calculation of local Poiseuille flow in a channel of rectangular cross-section. His solution modifies (A 4) to

$$\partial P/\partial \xi = -[(n+1)/n]\,\mathscr{Q}/H^3, \tag{B 1}$$

where n is a function of aspect ratio determined by

$$n(n+1) = (\tfrac{1}{2})\,(w/h)^2. \tag{B 2}$$

Second, the theory of appendix A overlooks the presence of the inactive channels near the moving seals. We deal with this approximately by supposing that the pump comprises two passages in parallel: (i) the quasi-two-dimensional active channel in which peristaltic waves propel the fluid, and (ii) an inactive leakage channel of constant cross-sectional area (see figure 3).

If the minimum gap width in the active channel is not too small compared with the depth of the active channel, the pressure at any length co-ordinate ξ will be nearly identical in the active and inactive channels. We assume that this is true, thus neglecting the pressure variations required to force liquid between the two channels.

Let $Q(\xi, \tau)$ be the flow through the active channel, and let $Q_L(\xi, \tau)$ be the flow through the leakage channel; further, let

$$Q_{\text{net}}(\xi, \tau) = Q + Q_L \tag{B 3}$$

be the net instantaneous flow through the machine at the position ξ.

The total local cross-sectional area at any instant is

$$A_{\text{net}}(\xi, \tau) = 2wh + A_L, \tag{B 4}$$

where A_L is the inactive leakage area. Now, defining

$$\mathscr{Q}_{\text{net}} \equiv Q_{\text{net}}/2wac \quad \text{and} \quad \mathscr{Q} \equiv Q/2wac,$$

(B 3) may be written as

$$\mathscr{Q}_{\text{net}} = \mathscr{Q} + \frac{A_L}{2aw}\left(\frac{Q_L}{A_L c}\right). \tag{B 5}$$

Noting that A_L is a constant, the equation of continuity is written as

$$\partial \mathscr{Q}_{\text{net}}/\partial \xi + \partial H/\partial \tau = 0. \tag{B 6}$$

Assuming, as before, a travelling wave, $H = H(\xi - \tau)$, (B 6) may be expressed as

$$\partial \mathscr{Q}_{\text{net}}/\partial \xi = \partial H/\partial \xi, \tag{B 7}$$

which, upon integration with respect to ξ, yields

$$\mathscr{Q}_{\text{net}} = H + f(\tau). \tag{B 8}$$

We now assume that the flow in the leakage channel is also inertia-free. Using the original premise that the two channels experience the same pressure gradient, it follows that Q_L is proportional to $\partial P/\partial \xi$. Using dimensional arguments, this is expressed as

$$\frac{Q_L}{A_L c} = -K \frac{A_L}{a^2} \frac{\partial P}{\partial \xi}, \tag{B 9}$$

where K is a pure positive number whose magnitude depends only on the cross-sectional shape of the leakage channel. If the latter were circular, for instance, K would have the value $\frac{3}{8}\pi$. Elimination of $\partial P/\partial \xi$ from (B 1) and (B 9) produces

$$\frac{Q_L}{A_L c} = \frac{n+1}{n} \frac{K A_L/a^2}{H^3} \mathscr{Q}. \tag{B 10}$$

Substituting this value of $Q_L/A_L c$ into (B 5) then leads to

$$\mathscr{Q}_{\text{net}} = \mathscr{Q}\left(1 + \frac{n+1}{n} \frac{\mathscr{C}}{H^3}\right), \tag{B 11}$$

where $\mathscr{C}$ is a pure number having the character of a conductance, and is defined by

$$\mathscr{C} \equiv K A_L^2/2a^3 w. \tag{B 12}$$

Substituting for $\mathscr{Q}$ from (B 11) into (B 1), and using (B 8), we get

$$\frac{\partial P}{\partial \xi} = -\frac{\mathscr{Q}_{\text{net}}}{[n/(n+1)]H^3 + \mathscr{C}} = -\frac{H}{[n/(n+1)]H^3 + \mathscr{C}} - \frac{f(\tau)}{[n/(n+1)]H^3 + \mathscr{C}}. \tag{B 13}$$

Integrating over the dimensionless distance $\mathscr{L}$ between the end reservoirs, and noting that $d\xi = d(\xi - \tau)$ for an integration at constant time, we obtain

$$-\Delta P_{\mathscr{L}} = \int_0^{\mathscr{L}} \frac{H\, d(\xi - \tau)}{[n/(n+1)]H^3 + \mathscr{C}} + \int_0^{\mathscr{L}} \frac{f(\tau)\, d(\xi - \tau)}{[n/(n+1)]H^3 + \mathscr{C}}. \tag{B 14}$$

Now, both H and n are functions of the argument $(\xi - \tau)$. Therefore, if $\mathscr{L}$ is an integer (signifying an integral number of wavelengths between the reservoirs), and if the pressure difference $\Delta P_{\mathscr{L}}$ between the reservoirs is constant in time, study of (B 14) shows that $f(\tau)$ must in fact be a constant T. These are precisely the conditions of the experiments.

Taking the time-mean of (B 8), we may thereby arrive at

$$T = \bar{\mathscr{Q}}_{\text{net}} - \bar{H} = \mathscr{Q}_{\text{net}} - H; \tag{B 15}$$

thus (B 13) finally becomes

$$\frac{\partial P}{\partial \xi} = \frac{\bar{H} - \bar{\mathscr{Q}}_{\text{net}}}{[n/(n+1)]H^3 + \mathscr{C}} - \frac{H}{[n/(n+1)]H^3 + \mathscr{C}}, \tag{B 16}$$

which should be compared with (A 8). Note that $\bar{Q}_{\text{net}}$ is the time-mean flow measured in the experiments.

Integration of (B 16) for $\Delta\xi = 1$ gives the pressure rise per wavelength while integration for $\Delta\xi < 1$, with various values of τ, gives the pressure–time relationship at the location $\Delta\xi$ downstream of a pressure node. The integrations must be performed numerically.

REFERENCES

BURNS, J. C. & PARKES, T. 1967 Peristaltic motions. *J. Fluid Mech.* **29**, 731–743.

ECKSTEIN, E. C. 1970 Experimental and theoretical pressure studies of peristaltic pumping. S.M. thesis, M.I.T.

FUNG, Y. C. & YIH, C. S. 1968 Peristaltic transport. *J. Appl. Mech.* **35**, 669–675.

FUNG, Y. C. & YIH, C. S. 1969 Closure of Jaffrin & Shapiro (1969).

HANIN, M. 1968 The flow through a channel due to transversely oscillating walls. *Israel J. Technol.* **6**, 67–71.

JAFFRIN, M. Y. 1971 Inertia and streamline curvature effects on peristaltic pumping. *Proc. 7th Annual Mtg of Soc. of Eng. Sci.* (To be published.)

JAFFRIN, M. Y. & SHAPIRO, A. H. 1969 Discussion of Fung & Yih (1968). *J. Appl. Mech.* **36**, 279–281.

LATHAM, T. W. 1966 Fluid motions in a peristaltic pump. S.M. thesis, M.I.T.

PURDAY, H. F. P. 1949 *An Introduction to the Mechanics of Viscous Flow.* Dover.

SHAPIRO, A. H. 1967 Pumping and retrograde diffusion in peristaltic waves. *Proc. Workshop on Ureteral Reflux in Children.* Washington, D.C.: Nat. Acad. Sci.

SHAPIRO, A. H., JAFFRIN, M. Y. & WEINBERG, S. L. 1969 Peristaltic pumping with long wavelengths at low Reynolds number. *J. Fluid Mech.* **37**, 799–825.

WEINBERG, S. L. 1970 A theoretical and experimental treatment of peristaltic pumping and its relation to ureteral function. Ph.D. thesis, M.I.T.

YIN, F. & FUNG, Y. C. 1969 Peristaltic waves in circular cylindrical tubes. *Trans. ASME* **36**E, 579–587.

ZIEN, T. F. & OSTRACH, S. 1970 A long wave approximation to peristaltic motion. *J. Biomech.* **3**, 63–75.

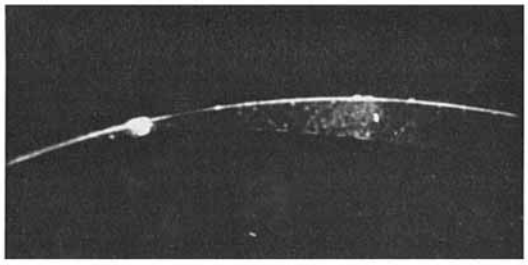

(*a*)

(*e*)

(*b*)

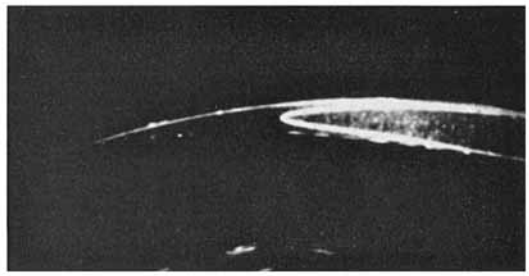

(*f*)

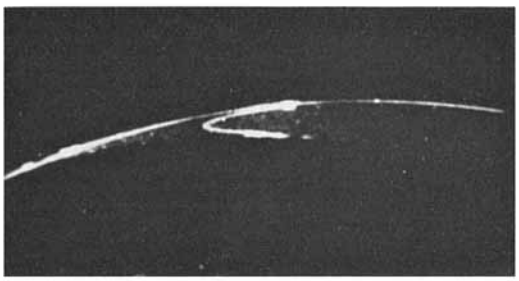

(*c*)

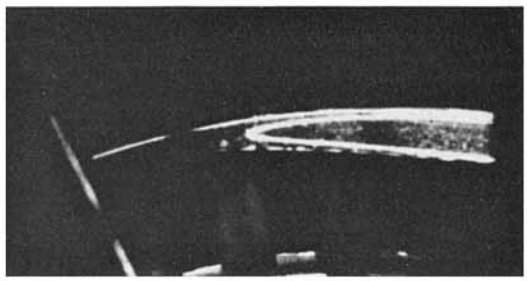

(*g*)

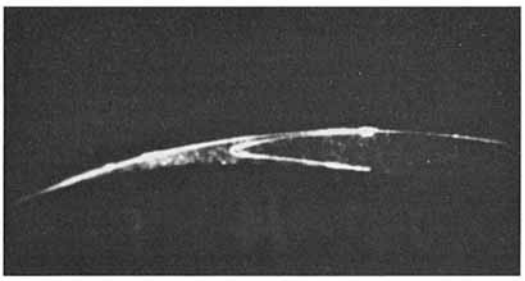

(*d*)

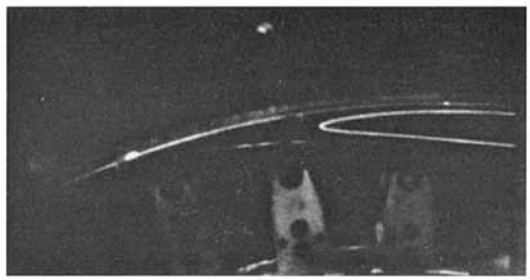

(*h*)

FIGURE 8. Cine frames for $\phi = 0{\cdot}7$, $\bar{\mathcal{Q}}/\bar{\mathcal{Q}}_0 = 1$. Dye originally injected *outside* trapped bolus ultimately approximates the shape of the split stagnation streamline (see Weinberg). τ: (*a*) 0; (*b*) 0·066; (*c*) 0·204; (*d*) 0·287; (*e*) 0·368; (*f*) 0·532; (*g*) 0·695; (*h*) 1·190.

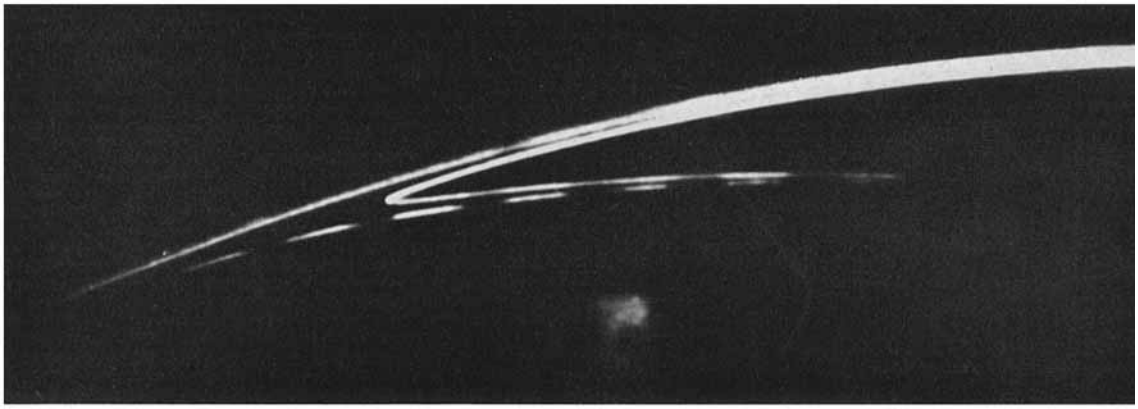

(*a*)

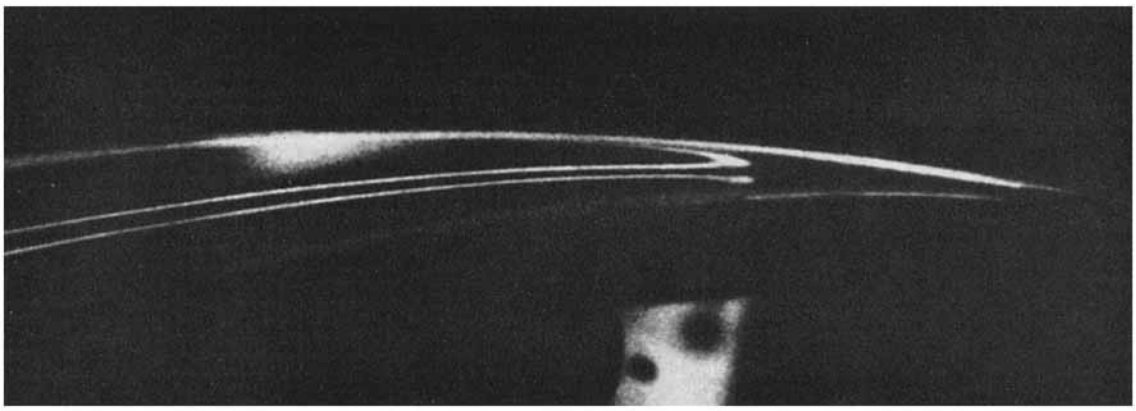

(*b*)

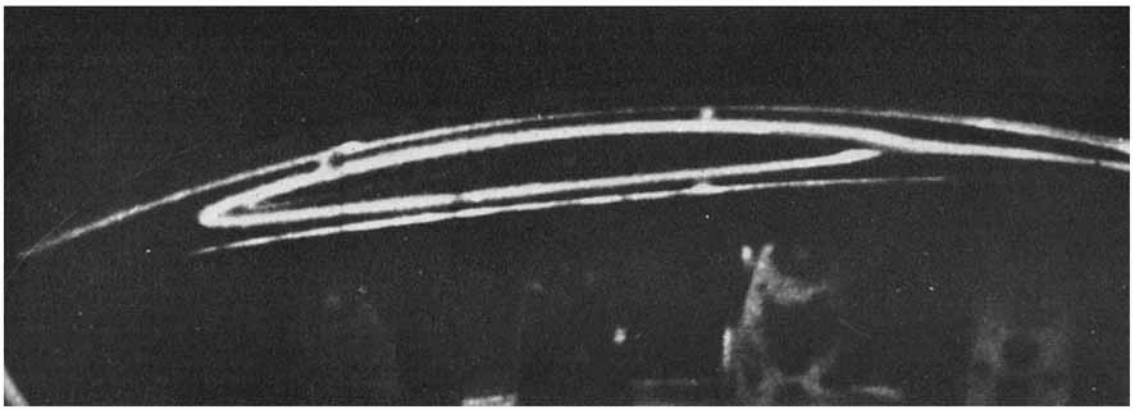

(*c*)

FIGURE 9. Cine frames for experiments with $\bar{\mathcal{Q}}/\bar{\mathcal{Q}}_0 = 1$. Dye is originally injected *inside* the trapped bolus and ultimately approximates the split stagnation streamline. (*a*) Leading edge of bolus. (*b*) Internal streamline pattern. (*c*) Overall view of bolus. (*a*), (*b*) $\phi = 0{\cdot}9$; (*c*) $\phi = 0{\cdot}7$. (See Weinberg.)